Published in final edited form as:

Clin Cancer Res. 2020 November 15; 26(22): 6051–6063. doi:10.1158/1078-0432.CCR-20-1359.

CXCR3 and Cognate Ligands are Associated with Immune Cell Alteration and Aggressiveness of Pancreatic Ductal Adenocarcinoma

Andrew Cannon[1], **Christopher M. Thompson**[1], **H. Carlo Maurer**[2,3,4], **Pranita Atri**[1], **Rakesh Bhatia**[1], **Sean West**[5], **Dario Ghersi**[5], **Kenneth P. Olive**[2,3], **Sushil Kumar**[1], **Surinder K. Batra**[1,6]

[1]Department of Biochemistry and Molecular Biology, University of Nebraska Medical Center, Omaha, Nebraska

[2]Department of Medicine, Columbia University Irving Medical Center, New York, New York

[3]Herbert Irving Comprehensive Medical Center, New York, New York

[4]Klinikum rechts der Isar, II. Medizinische Klinik, Technische Universität München, Munich, Germany

[5]College of Information Science and Technology, University of Nebraska at Omaha, Omaha, Nebraska

[6]Fred and Pamela Buffet Cancer Center, University of Nebraska Medical Center, Omaha, Nebraska

Abstract

Purpose: The cytokine milieu in pancreatic ductal adenocarcinoma (PDAC) promotes tumor progression and immune suppression, contributing to the dismal prognosis of patients with PDAC. The roles of many of these cytokines, however, have not been thoroughly investigated in PDAC.

Experimental Design: PDAC microarray and The Cancer Genome Atlas datasets were analyzed to identify cytokines and cognate receptors overexpressed in PDAC and associated with survival. Pathway and CIBERSORT analyses were used to elucidate potential mechanisms of altered patient survival. Comparative analysis of cytokine expression in KPC (K-ras^{G12D}; TP53^{R172H}; Pdx-1cre) and KC (K-ras^{G12D}; Pdx-1cre) PDAC models and multicolor

Corresponding Authors: Surinder K. Batra, University of Nebraska Medical Center, 42nd and Emile, 7054, Omaha, NE 68198. Phone: 402-559-7754; Fax: 402-559-6650; sbatra@unmc.edu; and Sushil Kumar, Phone: 402-559-3138, Fax: 402-559-6650; skumar@unmc.edu.

Authors' Contributions

A. Cannon: Conceptualization, software, formal analysis, investigation, methodology, writing-original draft. **C.M. Thompson:** Software, formal analysis, investigation, methodology. **H.C. Maurer:** Software, investigation, methodology. **P. Atri:** Software, investigation, methodology. **R. Bhatia:** Investigation, methodology. **S. West:** Software, investigation, methodology. **D. Ghersi:** Conceptualization, supervision, methodology. **K.P. Olive:** Software, supervision, investigation. **S. Kumar:** Conceptualization, supervision, methodology, writing-original draft. **S.K. Batra:** Conceptualization, supervision, writing-original draft.

Disclosure of Potential Conflicts of Interest

S.K. Batra is co-founder of Sanguine Diagnostics and Therapeutics, Inc. No potential conflicts of interest were disclosed by the other authors.

Note: Supplementary data for this article are available at Clinical Cancer Research Online (http://clincancerres.aacrjournals.org/).

immunofluorescence (IF) staining of human PDAC–resected samples were used to validate these findings.

Results: *CXCL9* and *CXCL10* were among the most highly overexpressed cytokines by bioinformatics analyses, while their receptor, CXCR3, was significantly overexpressed by IHC analysis. Higher CXCR3 ligand expression was associated with shorter overall survival, while high *CXCR3* expression was associated with better survival. The CXCR3 ligands, *CXCL4, 9*, and *10*, were overexpressed in KPC compared with KC mice. Pathway analysis of CXCR3- and CXCR3 ligand–associated genes showed that *CXCR3* is a marker of antitumor immunity, while its ligands may promote immunosuppression. CIBERSORT and IF studies of PDAC tissues demonstrated that high CXCR3 expression was associated with increased $CD8^+$ T-cell and naïve B-cell signatures and loss of plasma cell signatures. CXCR3 ligand expression was associated with increased $CD8^+$ T-cell signatures and loss of natural killer–cell signatures.

Conclusions: CXCR3 ligands are overexpressed in PDAC and are associated with poor survival likely related to alterations in tumor immune infiltrate/activity.

Introduction

Pancreatic ductal adenocarcinoma (PDAC) is among the most aggressive human malignancies, with nearly 80% of patients being diagnosed with late-stage disease and a 5-year overall survival (OS) rate of 9%. PDAC development is facilitated by an inflammatory microenvironment through NFATC1/2 (1, 2), NFκB (3), and WNT/β-catenin–mediated signaling. These pathways provide a survival advantage by preventing cancer cell apoptosis and senescence (4, 5), and increasing epithelial-to-mesenchymal transition (6). In addition, inflammation indirectly influences tumor progression by modulating tumor immune infiltrates, resulting in suppression of antitumor immunity. Mechanisms of reducing antitumor immunity include expansion of regulatory T cells (Treg; ref. 7), recruitment of immunosuppressive myeloid cells (8–10), as well as increased expression of immune checkpoint molecules (11), and promotion of ineffective Th2-mediated/humoral response (9).

Cytokines and chemokines serve as key regulators of cancer biology and inflammatory response. For instance, IL6 induces cancer cell invasion and sustains the proliferative potential of PDAC cells (12, 13), while it suppresses Th1 polarization in favor of Th17 (14, 15). Similar dual roles have been reported for CXCR2 ligands (16, 17), CXCL12 (18, 19), and LIF (20, 21) in PDAC, suggesting that numerous cytokines play a critical role in cancer biology and immune response during cancer progression.

We used human PDAC microarray and The Cancer Genome Atlas (TCGA) datasets to determine the relative expression of 149 cytokines/chemokines in PDAC compared with the normal pancreas and confirmed expression of their cognate receptors. In combination, these analyses showed that CXCR3 ligands are among the most highly and consistently overexpressed cytokines in human PDAC, and CXCR3 is expressed in the epithelial and stromal compartments of PDAC tumors. We focused further analyses on CXCR3 and its ligands, as their functions are poorly defined in PDAC. CXCR3 is a G protein–coupled receptor of ELR-negative CXC-motif–containing chemokines CXCL9, CXCL10, CXCL11,

PF4 (CXCL4), and PF4V1 (CXCL4L1; refs. 22–24). Two splice variants of CXCR3, CXCR3A and CXCR3B, have differential expression in PDAC with markedly different biology. CXCR3A, primarily expressed on T cells, has a high affinity for CXCL9, 10, and 11 and mainly signals through the activation of $G\alpha_i$, leading to inhibition of adenylate cyclase (22, 25). In contrast, CXCR3B is expressed predominantly on endothelial cells and binds PF4 with high affinity. Importantly, CXCR3B activates $G\alpha_s$ and thereby, stimulates adenylate cyclase. In PDAC, PF4V1/CXCR3A signaling was associated with modestly increased invasion in subcutaneous implantation models of PDAC. In addition, *CXCR3* and *CXCL10* levels correlated with the expression of several T-cell–related genes in PDAC (26). While these studies provide some insight into the function of CXCR3 and its ligands in PDAC, no study has comprehensively addressed the expression and function of CXCR3 splice variants and their ligands in PDAC.

We further utilized pathway, gene set enrichment (GSE), and CIBERSORT analyses, to provide insight into the mechanism through which the CXCR3 axis is associated with PDAC patient outcomes. In addition to demonstrating that *CXCL9* and *CXCL10* are consistently overexpressed in PDAC, we showed that CXCR3A and B ligands were independently associated with poor outcomes in PDAC. In contrast, expression of either *CXCR3* splice variant was associated with improved overall survival (OS). Interestingly, pathway, GSE, and CIBERSORT analyses suggested that *CXCR3* splice variants and CXCR3A ligands were associated with altered tumor immune infiltrates, and CXCR3A ligands were associated with gene signatures consistent with immunosuppression.

Materials and Methods

Ethics and rigor

The research presented here was conducted in accordance with the U.S. Common Rule. Use of animals was approved by the Institutional Animal Care and Use Committee at University of Nebraska Medical Center (Omaha, Nebraska). Randomization, blinding, and power analyses were not conducted given the retrospective nature of the study.

Microarray data

PDAC microarray datasets that contain tumor and normal (adjacent or otherwise) samples were queried and downloaded through NCBI Gene Expression Omnibus. The GSE15471 (ref. 27; $n = 36$ paired samples), GSE16515 (ref. 28; $n = 36$ tumor and 16 normal samples), GSE18670 (ref. 29; $n = 6$ paired samples), GSE32676 (ref. 30; $n = 25$ tumor and 7 normal samples), GSE28735 (ref. 31; $n = 45$ paired samples), and GSE62452 (ref. 32; $n = 24$ tumor and 16 normal samples) were included in our analysis. In total, 172 tumors and 126 normal samples were compared across different microarray sets. The CEL files were Robust Multi-array Average (RMA) normalized and aggregated using Bioconductor AFFY package and R 3.6.1. The fold change (FC) was calculated for each tumor sample for all cytokines in each microarray dataset independently using the following equation:

$$FC_{Xiy} = 2^{X_{Ti} - \bar{X}_N}$$

where, FC_{Xiy} is the FC of gene X in the ith tumor sample in the yth dataset, X_{Ti} is the expression of X in the ith tumor sample, and $\overline{X}_N$ is the mean expression of X in normal samples. Concordantly, reported mean FC values are given by the following equation:

$$\overline{FC_{Xy}} = \frac{\sum_{i=1}^{n} FC_{Xiy}}{n}$$

where, $\overline{FC_{Xy}}$ is the mean FC of gene X in the yth dataset, and n is the number of tumor samples. Heatmaps of cytokine/chemokine gene expression were constructed using the Bioconductor Complex-Heatmap package. For visual clarity, genes with mean FCs greater than 1.5 or less than 0.75, across arrays of a single platform type, were included in heatmaps.

TCGA dataset

The PAAD TCGA raw RNA-sequencing (RNA-seq) dataset was downloaded from TCGA website and normalized using the transcripts per million (TPM) method (33). For *CXCR3* splice variant quantification, BAM files were reverted to fastq format and remapped to the human reference genome (Ensembl 94, cDNA library) using Salmon with default parameters, allowing virtual recreation of full transcripts and thus, discrimination between *CXCR3A* and *B* variants (34, 35). Of the 182 patient samples in the PDAC dataset, only 140 patient samples with primary PDAC diagnosis and greater than 1% malignant cellularity were included in our analysis.

Columbia University Medical Center micro-dissected PDAC dataset

A total of 123 samples from patients who underwent surgery at Columbia Pancreas Center were acquired with appropriate consent (36). The cryosections of each sample were prepared and stained with Cresyl violate acetate. Stained sections were micro-dissected to acquire at least 1,000 cells per compartment. Paired micro-dissected PDAC epithelial and stromal samples were analyzed by RNA-seq performed at Columbia University Medical Center (CUMC; New York, NY). Reads were mapped to the human genome, and expression data were TPM normalized (36). These data were queried for expression of *CXCR3* and CXCR3 ligands in stromal and epithelial compartments.

Survival analysis

Kaplan–Meier survival analysis was implemented in JMPpro 14 for *CXCR3* splice variants, CXCR3A ligands, *PF4*, and *PF4V1*. Multiple points of stratification were used for each gene. For the initial stratification, high and low expression groups were defined by the median expression of the gene/gene set. In the second round, very high expression (≥75th percentile) was compared with low expression (≤75th and 50th percentile). In the third round, high expression (≥50th percentile) was compared with very low expression (≤25th percentile). The lowest calculated *P* value is depicted for genes with insignificant comparisons for all stratification points. Because of its potential importance in both cancer cells as well as stromal cells, we stratified patients by median *CXCR3A* expression and

cellularity. Subsequently, we analyzed survival associations in high- and low-cellularity groups.

Cytokine PCR array

KC (K-ras^{G12D}; Pdx-1cre) and KPC (K-ras^{G12D}; TP53^{R172H}; Pdx-1cre) mice and their respective wild-type (WT) littermates (n = 6 for each group) were profiled for cytokine expression at histologically matched 25–30 and 10–15 weeks of age, respectively (Supplementary Fig. S1). RNA was isolated from the pancreas of each mouse, pooled, and used as a template (1 μg) for the first-strand synthesis. The Qiagen qRT-PCR Array (PAMM150Z, SA Bioscience) was performed in triplicate according to the manufacturer's instructions. Data were normalized to a panel of house-keeping genes, and differential gene expression, relative to WT littermates, was calculated using the Qiagen webserver. The FC values returned by the Qiagen webserver were subsequently compared between KC and KPC animals.

Pathway analysis

Spearman ρ correlation coefficients and corresponding P values between *CXCR3A* total and high- and low-cellularity subgroups; *CXCR3B*; the linear combination of *CXCL9, 10, 11; PF4; PF4V1*; and each gene in the previously described subset of the PDAC TCGA samples were calculated. Correlations with P values less than 0.001 were included for further analysis. Significant correlations for each gene were divided into positive and negative sets based on the sign of ρ. The genes in each set were analyzed using ingenuity pathway analysis (IPA; ref. 37) and the top 10 significant pathways by IPA were considered for each gene/set of genes analyzed.

Splenocyte isolation, activation, and qPCR for markers of T-cell exhaustion

Splenocytes harvested from male and female, 8- to 10-week-old C57/BL6 mice were plated (2×10^6) in a 24-well plate in 1 mL of media. To activate the T cells, splenocytes were treated with anti-CD3e antibody (1.5 μL/mL, Invitrogen, Clone 145–2C11), anti-CD28 antibody (2.0 μL/mL, Invitrogen, Clone 37.51), murine IL2 (200 U/mL, PeproTech), and TGFβ1 (3 ng/mL, PeproTech). Activation state was confirmed by flow cytometry for CD25$^+$ cells (Supplementary Fig. S2). Cells were subsequently treated with vehicle control (water with 1% BSA) or 100 ng/mL of Cxcl10 (PeproTech). After 96 hours, cells were harvested, lysed, and RNA was extracted. The cDNA was synthesized using 0.5 μg of RNA along with iScript first-strand synthesis kits and qRT-PCR for *LAG3, CTLA4*, and *CD274* (PD-L1), markers of T-cell exhaustion highlighted by IPA, was performed.

CIBERSORT analysis

Quantification of relative immune cell gene expression signatures for 22 immune cell types in the 140 primary PDAC samples in the PAAD TCGA dataset was calculated using CIBERSORT and the LM22 signature matrix (38). The LM22 matrix is a gene signature matrix composed of the gene signatures of 22 immune cell types derived from microarray analysis of flow cytometry–sorted or cell culture–differentiated cell populations. Samples were subsequently stratified by median expression for *CXCR3A* and *B* and the sum of

CXCL9, 10, and *11*, as in survival analysis. In addition, for the analysis of *CXCR3A*, samples were stratified by cellularity and *CXCR3A* expression (as in survival analysis). Mann–Whitney U tests were used to compare the distributions of immune cell infiltrate scores of high- and low-expression groups for *CXCR3* splice variants and CXCR3A ligands, with a *P* value less than 0.05 being significant.

IHC and immunofluorescence analysis

For IHC, deidentified primary PDAC ($n = 40$ Whipple and $n = 21$ Rapid autopsy) tissue sections [institutional review board exempted under 45CFR46.102(f), Office of Regulatory Affairs] were stained with anti-CXCR3 antibody (1:200 mab160, R&D Systems) as described previously (39). Briefly, tissues were hydrated, incubated for 1 hour in 0.3% hydrogen peroxide, followed by antigen retrieval in 10 mmol/L sodium citrate, pH 6.0 for 15 minutes. The sections were blocked in 2.5% Horse Serum (Vector Laboratories) for 1 hour at room temperature and incubated with primary antibody overnight at 4°C. Universal secondary antibody (Vector Laboratories) was incubated on the slide for 1 hour at room temperature and developed for 2 minutes with the DAB Substrate (Vector Laboratories). Slides were counterstained with hematoxylin and mounted in Permount.

For immunofluorescence (IF) staining, primary PDAC samples ($n = 23$) were stained with anti-CXCR3 (1:200, mab160, R&D Systems), anti-CD8 (1:100, AMC908, Thermo Fisher Scientific), CD20 (1:100, D-10, Santa Cruz Biotechnology), and CD138 (1:100, PA5–16918, Thermo Fisher Scientific). Specimens were blocked with 10% normal goat serum (NGS) in TBS-TX for 1 hour at room temperature and incubated with CXCR3 and CD138 antibodies in 10% NGS overnight at 4°C. Slides were incubated with AlexaFluor-405 anti-mouse IgG and AF-568 anti-rabbit IgG antibodies at a 1:400 dilution in 10% NGS for 1 hour at room temperature, washed three times for 10 minutes each, and reblocked for 20 minutes in 10% NGS. Following the second blocking, slides were stained with fluorophore-conjugated primary antibodies against CD8 (AlexaFluor-488) and CD20 (AlexaFluor-647) in 10% NGS for 6 hours and washed three times for 10 minutes each in TBS-TX. Slides were incubated briefly with Tru Black (autofluorescence quenching agent, Biotium) for 1 minute followed by mounting in an aqueous mounting medium. Stained slides were imaged on a Zeiss LSM 800 Confocal Microscope at 400× magnification, and images of 10 high-power fields were acquired per specimen and processed using Zen Blue Software (Zeiss) to produce negative staining in normal human cerebral cortex and positive staining in secondary lymphoid organs. For CXCR3, CD8, and CD138 staining, individual cells with signal exceeding the level of background correction that were not of obvious epithelial origin were manually counted as positive for that marker. Cellular immunophenotypes ($CD8^+CXCR3^+$, $CD8^+CXCR3^-$, $CXCR3^+CD8^-$, and $CD138^+$) were recorded. Specific CD20 staining was strongly associated with lymphoid aggregates, therefore, we quantified lymphoid aggregates using ImageJ. Briefly, for each section, 100× images encompassing the entirety of each lymphoid aggregate were captured and pixel area was quantified using ImageJ. Samples were stratified on the basis of the median number of $CXCR3^+$ cells per field, and number of $CD8^+$ and $CD138^+$ cells, as well as the lymphoid aggregate area, were compared across CXCR3 high and low groups using Mann–Whitney U tests.

Results

Analysis of cytokine expression in PDAC

Using four GPL570 and two GPL6244 PDAC microarray datasets (172 tumor and 126 normal tissues), we analyzed the relative expression of 149 cytokines/chemokines genes. In GPL570 arrays, 40 cytokines were identified as having a mean FC greater than 1.5 or less than 0.75 (Fig. 1A). Furthermore, results with probes measuring the expression of the same cytokine strongly agreed, suggesting accurate quantification of expression. In addition to confirming upregulation of CXCR1/2 ligands *CXCL1, CXCL3, CXCL5*, and *CXCL8 (IL8)*; *LIF*; and *CXCL13*, we also demonstrated that *CXCR3* ligands *CXCL9* (mean FC, 2.30; *P* values for four microarrays, 6.8×10^{-5}, 0.14, 0.388, and 0.68), *CXCL10* (mean FC, 3.2; $P = 2.3 \times 10^{-5}$, 3.6×10^{-4}, 0.0877, and 0.5), and *CXCL11* (mean FC, 2.35; $P = 0.066$, 0.955, 0.18, and 0.12), were consistently overexpressed in GPL570 microarrays. *TNFSF8, CXCL12*, and *CSF3* were the only cytokines consistently downregulated in PDAC tissues. Two additional arrays from the GPL6244 platform, GSE28735 and GSE62452, showed 21 cytokines differentially regulated between tumor and normal. Of these 21 genes, 20 genes were common between GPL570 and GPL6244 arrays including *CXCL5, CXCL8, CXCL12*, and *LIF* (Fig. 1B and C). Importantly, *CXCL9* (mean FC, 1.90; *P* values for both arrays, 0.015 and 0.004) and *CXCL10* (mean FC, 2.96; $P = 0.001$ and 0.001) were significantly upregulated in both arrays, further highlighting the potential importance of these CXCR3 ligands in PDAC (Fig. 1B).

We next determined the *CXCR3* ligand expression profile in PDAC tissue in microarray and RNA-seq datasets (Fig. 1D–G). The pattern of *CXCR3* ligand expression was highly consistent, with *PF4V1* having substantially lower expression than the other four ligands ($P = 2.2 \times 10^{-16}$ *PF4* vs. *PF4V1* in TCGA), while *CXCL9* and *CXCL10* showed the highest expression. Importantly, this pattern was consistent across two microarray platforms and RNA-seq datasets. Next, we examined the cellular origin of *CXCR3* ligands using micro-dissected RNA-seq data from 123 paired epithelial and stromal samples from patients with PDAC (Fig. 1H and I). *CXCL9* and *10* were largely derived from the stromal compartment ($P = 5.0 \times 10^{-10}$ and 9.5×10^{-10}, respectively), while *CXCL11* was derived nearly equally from epithelium and stroma. *PF4* and *PF4V1* were expressed to a slightly greater extent in epithelial samples. In TCGA, *CXCL9* and *10* had significantly higher expression in low-cellularity samples, supporting the results from the CUMC dataset (Supplementary Fig. S3).

Assessment of CXCR3 expression in PDAC

We used microarray and RNA-seq resources to assess CXCR3 expression in PDAC. *CXCR3* was expressed in all samples analyzed by microarray, and expression was higher in the four GPL570 arrays (Fig. 2A) compared with the GPL6244 arrays (Fig. 2B). Because the biology of CXCR3 signaling is dependent on its splice variants, we used TCGA RNA-seq data to quantify the expression of *CXCR3* splice variants by a stringent mapping of reads to generate virtual recreations of full transcripts (Fig. 2C). As in the microarray data, *CXCR3* was expressed in the majority of PDAC samples, and *CXCR3A* was the predominant splice variant ($P = 2.2 \times 10^{-16}$). To delineate the cellular origin of *CXCR3* transcripts, we queried CUMC RNA-seq data (Fig. 2D) and found that *CXCR3* was expressed in the majority of

samples (108/123) in both epithelial (73/123) and stromal (94/123) compartments. Expression of *CXCR3* was substantially higher in the stromal compartment (median TPM all, 0.543 vs. 2.6; median TPM *CXCR3*$^{+}$, 2.76 vs. 5.98 for epithelial and stromal expression, respectively). These findings are consistent with the association of higher *CXCR3* expression in low-cellularity samples (Supplementary Fig. S4). Interestingly, few tumors showed balanced *CXCR3* expression ($P < 0.004$) in both epithelial and stromal compartments (Fig. 2E).

To validate our findings in microarray and RNA-seq datasets, we stained human and murine PDAC tissues for CXCR3. CXCR3 expression was minimal in the pancreata of 7- and 25-week-old WT mice. In KPC mice, robust CXCR3 expression was observed in both compartments by 25 weeks (Fig. 2F), suggesting that CXCR3 expression increases with disease progression. Similarly, in human samples ($n = 21$), the normal pancreas expressed little to no CXCR3, but PDAC tissue showed robust CXCR3 expression (composite score = 11.3) in the malignant epithelium and associated stroma (Fig. 2G).

CXCR3 and CXCR3 ligand expression on OS in PDAC

To understand the role of CXCR3 ligands in PDAC outcomes, we performed Kaplan–Meier survival analyses in TCGA data stratified by the sum of CXCR3A ligand (*CXCL9, CXCL10,* and *CXCL11*), *PF4*, and *PF4V1* expression (Fig. 3A–C). The patients with high (stratified by median) CXCR3A ligand expression were associated with significantly worse survival (Fig. 3A). While stratification by median *PF4* expression was not significant, the top 25% expressers had significantly poorer survival compared with the lowest 50% and 75% expressers (Fig. 3B and C; Supplementary Fig. S5).

Similarly, we conducted a survival analysis on the high and low expression of *CXCR3* splice variants. When stratified by the median, high *CXCR3B*-expressing patients had significantly better OS, while *CXCR3A* expression did not reach significance (Fig. 3D and E). Because *CXCR3A* can be expressed in different tumor compartments, we assessed *CXCR3A* expression in PDAC samples stratified by median cellularity and *CXCR3A* expression. Importantly, in the high epithelial cellularity group, high C*XCR3A* expression trended toward worse OS; however, in the low-cellularity group, high *CXCR3A* expression correlated with improved OS, suggesting that *CXCR3A* has different prognostic importance depending on compartment-specific expression (Fig. 3F and G).

Finally, we performed a cytokine qRT-PCR array in two murine models of PDAC with markedly different phenotypes at histologically matched timepoints. The KPC represents a highly aggressive model, while the KC represents a disease that is more indolent with lower penetrance. In comparing the cytokines that were differentially expressed at a histologically similar stage (Supplementary Fig. S1), in each of these models relative to WT littermates, *Cxcl10* and *Pf4* were upregulated specifically in the more aggressive KPC model (Fig. 3H). Notably, *Cxcl9* also had higher expression in KPC tumors relative to KC tumors (Fig. 3H). In sum, these results suggest that the CXCR3 axis is upregulated specifically in the more aggressive model and may contribute to this aggressive phenotype.

Pathway analysis of CXCR3- and CXCR3 ligand–correlated genes

We used Spearman correlations to generate sets of genes significantly correlated with the expression of CXCR3A ligands, *PF4* and *PF4V1*, and *CXCR3* splice variants in TCGA dataset. These gene sets were analyzed via IPA. First, gene sets associated with *CXCR3A* and *B* expression were most enriched for T-cell–related pathways (Fig. 4A and B). In addition, T-cell–related pathways were more prominently enriched in low-cellularity samples as compared with high-cellularity samples (Fig. 4C and D). T-cell–related genes were also prominently correlated with *CXCL9, 10*, and *11* expressions (Fig. 4E). Notably, T-cell exhaustion, PD-1, and PD-L1 pathways appeared as top hits only for the gene set correlated with *CXCL9, 10*, and *11* expression (Fig. 4E). These findings were supported by identical analyses conducted using microarray data and were consistent using different *P*-value cutoffs for inclusion and exclusion of correlations (Supplementary Data S1). Finally, the pathways associated with *PF4* and *PF4V1* expression were very distinct from each other and those associated with the receptors and CXCR3A ligands (Fig. 4F and G). Consistent with these findings, we found that *ex vivo* treatment of murine splenocytes with CXCL10 augmented the expression of immunosuppressive markers *LAG3, CTLA4*, and *CD274*, which were also highlighted in the IPA analysis (Fig. 4H). Using GSEA (40) on TCGA data, high expression of *CXCR3A* and *CXCL9, 10*, and *11* were both significantly associated with immune-related gene sets and consistent with IPA; *CXCL9, 10*, and *11* associated more closely with immunosuppressive gene sets than *CXCR3A* (Supplementary Fig. S6).

CIBERSORT of PDAC samples stratified by CXCR3 and CXCR3 ligand expression

We used CIBERSORT and the LM22 gene signature matrix to investigate the association of *CXCR3* and its ligands with relative immune cell frequencies in the tumor. Within TCGA dataset, MΘ and M2 macrophages and CD4 memory T cells appeared to be the most abundant immune cells within the tumor (Fig. 5A). As with the survival analysis and GSEA, we stratified patients on the basis of the median expression of *CXCR3* splice variants and the sum expression of CXCR3A ligands and analyzed differences in immune cell signatures between high- and low-expression groups. MΘ gene signatures were decreased, while $CD8^+$ T cells were elevated in the groups expressing high *CXCR3B* (Fig. 5B), CXCR3A ligands (Fig. 5C), and *CXCR3A* (Fig. 6A). High expression of CXCR3A ligands was specifically associated with increased M1 gene signatures as well as the loss of natural killer (NK)-cell gene signatures compared with the low CXCR3A ligand expression (Fig. 5C; Supplementary Fig. S6). Importantly, these changes were consistent across microarray datasets (Supplementary Fig. S7). In high *CXCR3A*-expressing patients, we noted increased $CD8^+$ T-cell and naïve B-cell signatures and decreased plasma cell gene signatures compared with the low-expressing group (Fig. 6). When samples were stratified on the basis of sample cellularity and *CXCR3A* expression, as in the survival analysis, only patients with high *CXCR3A* and low cellularity demonstrated significant differences in immune cell subsets (Fig. 6). IF staining for CXCR3, CD8, and CD138, and quantification of the lymphoid aggregate area in resected PDAC patient samples (Whipple, $n = 23$) showed that the number of $CXCR3^+$ cells correlated significantly with $CD8^+$ cells and aggregate lymphoid area, which is indicative of B-cell content (Fig. 6D–F).

Discussion

The unbiased screen of relative expression of 149 cytokines in human microarray data elucidated numerous candidates of potential importance in the PDAC tumor microenvironment (TME). Among these, CXCR3 ligands, CXCL9 and CXCL10, were overexpressed in the PDAC microenvironment that is poorly investigated in PDAC biology. We found that CXCR3A ligands were predominately expressed by the stromal compartment, whereas PF4 and PF4V1 had higher expression in the epithelial compartment. Importantly, CXCR3 was also expressed in PDAC, both in the epithelial and stromal compartments, and CXC3A was the predominant variant. Previously, CXCR3 has been demonstrated to augment the expression of PD-L1 and PD-1, promote Treg polarization, drive B cell to plasma cell differentiation, and in several settings, support antitumor immune response (41–44). In addition, in melanoma, breast, and colon cancer, CXCR3 has been associated with increased metastasis independent of the immune response (45). The expression patterns we observed suggest CXCR3 mediates tumor–stromal cross-talk as well as stromal-specific signaling, which is consistent with the dual roles of CXCR3 found in other cancers.

Surprisingly, both variants of *CXCR3* and the *CXCR3* ligands had opposing associations with survival. *CXCR3*A expression was not significantly associated with survival in unselected patients. Still, in low-cellularity patients, in which a higher proportion of *CXCR3* expression is expected to come from the stroma, the survival difference was significant. These findings are highly consistent with an immune cell–mediated survival benefit associated with *CXCR3* expression. In contrast, in high-cellularity patients, the survival trend was reversed, however, not significantly. The pathway and GSE analyses further supported an immune-mediated survival benefit as high *CXCR3A* expression was associated with enrichment of immune-related gene sets. Furthermore, high *CXCR3A* expression correlated with increased populations of CD8 cells and B cells in CIBERSORT analysis. Previous reports have linked these immune cell types with increased survival both in CIBERSORT analyses of multiple cancers and through independent experimental quantification of immune cells in PDAC (46–48). Moreover, a recent study of immune infiltrates in hepatocellular carcinoma showed that plasma cell infiltrates were associated with suppressed antitumor immune response and more rapid tumor growth in mice (43). Here, we were able to validate the association of CXCR3 with the observed changes in all three immune cell populations using IF. Cumulatively, these studies support our hypothesis that CXCR3 expression is associated with altered immune cell infiltrates and that these alterations have biological and prognostic significance for patients with PDAC. The improved survival seen with high *CXCR3* expression seems to conflict with the poorer survival observed in high ligand-expressing patients. Pathway analysis, GSEA, and CIBEROSRT suggest high CXCR3A ligand expression is associated with an immune suppressive environment and loss of NK-cell signatures. Interestingly, *CXCR3B* expression was also associated with T-cell–related pathways even though only *CXCR3A* has been demonstrated to have a substantial expression on immune cells.

A study by Lunardi and colleagues found *in vitro* that coculture of PDAC cells with pancreatic stellate cells induced CXCL10 expression, primarily derived from pancreatic stellate cells. Our analysis of RNA-seq data from 123 micro-dissected PDAC samples

confirms a stromal origin of CXCL10 in human tumors. Lunardi and colleagues further showed that *CXCL10* was overexpressed by 2.18-fold, and high *CXCL10* expression was associated with poor prognosis, based on array data from 45 patients (26). The results from our study, in a much larger number of patients, support these findings with the addition that *CXCL9* is also highly overexpressed in the majority of PDAC samples. Finally, Lunardi and colleagues' study reported that several immune cell markers, including *FOXP3, CTLA4,* and *CD39* correlated with *CXCL10* and *CXCR3* expression in 32 or 34 of the original 45 PDAC samples. While these positive correlations were present in our analyses, they were identified as minor players in the pathway and CIBERSORT analyses leading to the identification of different immunosuppressive pathways. Moreover, the analysis of single-marker genes independently does not accurately quantify Treg infiltrate, thereby necessitating the utilization of more sophisticated methodologies.

Another study by Quemener and colleagues reported that *PF4V1* expression was higher compared with *PF4* in PDAC samples based on the qRT-PCR analysis (49). Our results from multiple large-scale gene expression datasets differed from this report, but were consistent across the microarray and RNA-seq platforms used, providing strong evidence that the expression of *PF4* is higher than that of *PF4V1* in PDAC. Our results suggest that the functional consequences of PF4V1 expression in PDAC may be limited because of its low expression in the majority of samples. Furthermore, PF4 binds CXCR3B with greater affinity than PF4V1 (22), and CXCL9, 10, and 11 all bind CXCR3A with greater affinity than PF4V1 (23); thus, the contributions of PF4 and CXCL9, 10, and 11 to PDAC biology may be even more significant. Finally, a recent article on CXCR3 in PDAC reported that CXCL10 derived from dorsal route ganglion neurons was involved in the recruitment of cancer cells to nerves, consistent with the finding from Quemener and colleagues (50). Interestingly, this study also found that neutralization of CXCL10 was associated with improved pain scores in mice; however, they did not observe differences in immune cell infiltrate (50). These findings do not contradict our observations, due to the fact that the expression of CXCR3A ligands was not associated with a paucity of immune cells, rather with an immunosuppressive gene signature, and second, Hirth and colleagues employed an antibody to neutralize CXCL10, whereas CXCL9 and CXCL11 were still active in the TME.

Overall, these analyses strongly suggested that CXCL9 and 10 are among the most highly and consistently overexpressed cytokines in PDAC, and the expression of these cytokines is associated with poor outcomes in patients with PDAC, potentially due to modulation of the immune microenvironment and exhaustion of T cells. Furthermore, CXCR3, the receptor for these two ligands, is expressed in PDAC in a spatiotemporal manner and is associated with improved outcomes. While the pathways correlated with *CXCR3* and CXCR3 ligand expression share some features, some associations were specific to each, potentially explaining how ligands and their receptor could have opposite associations with survival outcomes.

Supplementary Material

Refer to Web version on PubMed Central for supplementary material.

Acknowledgments

This work and/or authors were partly supported by funding from the NIH (P01CA217798 to S.K. Batra, U01 CA210240 to S.K. Batra, U01 CA200466 to S. K. Batra, R01 CA206444 to S.K. Batra, R21 AA026428 to S. Kumar, R01 CA228524 to S.K. Batra, F30 CA225117 to A. Cannon, and F31 CA243469 to C.M. Thompson). We are grateful to the UNMC Department of Pathology and Rapid Autopsy Program (Drs. Hollingsworth and Grandgenett) for providing pancreatic cancer patient samples. We are also thankful to Dr. Rachagani for his help in maintaining the pancreatic cancer murine models. We thank Dr. Jessica Mercer for editing the article.

References

1. Baumgart S, Chen NM, Siveke JT, Konig A, Zhang JS, Singh SK, et al. Inflammation-induced NFATc1-STAT3 transcription complex promotes pancreatic cancer initiation by KrasG12D. Cancer Discov 2014;4:688–701. [PubMed: 24694735]
2. Baumgart S, Chen NM, Zhang JS, Billadeau DD, Gaisina IN, Kozikowski AP, et al. GSK-3beta governs inflammation-induced NFATc2 signaling hubs to promote pancreatic cancer progression. Mol Cancer Ther 2016;15:491–502. [PubMed: 26823495]
3. Ying H, Elpek KG, Vinjamoori A, Zimmerman SM, Chu GC, Yan H, et al. PTEN is a major tumor suppressor in pancreatic ductal adenocarcinoma and regulates an NF-κB-cytokine network. Cancer Discov 2011;1:158–69. [PubMed: 21984975]
4. Guerra C, Collado M, Navas C, Schuhmacher AJ, Hernandez-Porras I, Canamero M, et al. Pancreatitis-induced inflammation contributes to pancreatic cancer by inhibiting oncogene-induced senescence. Cancer Cell 2011; 19:728–39. [PubMed: 21665147]
5. Rielland M, Cantor DJ, Graveline R, Hajdu C, Mara L, Diaz Bde D, et al. Senescence-associated SIN3B promotes inflammation and pancreatic cancer progression. J Clin Invest 2014;124:2125–35. [PubMed: 24691445]
6. Ren R, Yu J, Zhang Y, Wang SF, Guo X, Shen M, et al. Inflammation promotes progression of pancreatic cancer through WNT/β-catenin pathway-dependent manner. Pancreas 2019;48:1003–14. [PubMed: 31404031]
7. Mirlekar B, Michaud D, Searcy R, Greene K, Pylayeva-Gupta Y. IL35 hinders endogenous antitumor T-cell immunity and responsiveness to immunotherapy in pancreatic cancer. Cancer Immunol Res 2018;6:1014–24. [PubMed: 29980536]
8. Incio J, Liu H, Suboj P, Chin SM, Chen IX, Pinter M, et al. Obesity-induced inflammation and desmoplasia promote pancreatic cancer progression and resistance to chemotherapy. Cancer Discov 2016;6:852–69. [PubMed: 27246539]
9. De Monte L, Wormann S, Brunetto E, Heltai S, Magliacane G, Reni M, et al. Basophil recruitment into tumor-draining lymph nodes correlates with Th2 inflammation and reduced survival in pancreatic cancer patients. Cancer Res 2016;76:1792–803. [PubMed: 26873846]
10. Bayne LJ, Beatty GL, Jhala N, Clark CE, Rhim AD, Stanger BZ, et al. Tumor-derived granulocyte-macrophage colony-stimulating factor regulates myeloid inflammation and T cell immunity in pancreatic cancer. Cancer Cell 2012;21: 822–35. [PubMed: 22698406]
11. Lu C, Talukder A, Savage NM, Singh N, Liu K. JAK-STAT-mediated chronic inflammation impairs cytotoxic T lymphocyte activation to decrease anti-PD-1 immunotherapy efficacy in pancreatic cancer. Oncoimmunology 2017;6: e1291106. [PubMed: 28405527]
12. Grunwald B, Vandooren J, Gerg M, Ahomaa K, Hunger A, Berchtold S, et al. Systemic ablation of MMP-9 triggers invasive growth and metastasis of pancreatic cancer via deregulation of IL6 expression in the bone marrow. Mol Cancer Res 2016;14:1147–58. [PubMed: 27489361]
13. Ohlund D, Handly-Santana A, Biffi G, Elyada E, Almeida AS, Ponz-Sarvise M, et al. Distinct populations of inflammatory fibroblasts and myofibroblasts in pancreatic cancer. J Exp Med 2017;214:579–96. [PubMed: 28232471]
14. Delitto D, Delitto AE, DiVita BB, Pham K, Han S, Hartlage ER, et al. Human pancreatic cancer cells induce a MyD88-dependent stromal response to promote a tumor-tolerant immune microenvironment. Cancer Res 2017; 77:672–83. [PubMed: 27864347]

15. Hu W, Troutman TD, Edukulla R, Pasare C. Priming microenvironments dictate cytokine requirements for T helper 17 cell lineage commitment. Immunity 2011; 35:1010–22. [PubMed: 22137454]
16. Steele CW, Karim SA, Leach JDG, Bailey P, Upstill-Goddard R, Rishi L, et al. CXCR2 inhibition profoundly suppresses metastases and augments immunotherapy in pancreatic ductal adenocarcinoma. Cancer Cell 2016;29: 832–45. [PubMed: 27265504]
17. Chen L, Fan J, Chen H, Meng Z, Chen Z, Wang P, et al. The IL-8/CXCR1 axis is associated with cancer stem cell-like properties and correlates with clinical prognosis in human pancreatic cancer cases. Sci Rep 2014;4:5911. [PubMed: 25081383]
18. Ene-Obong A, Clear AJ, Watt J, Wang J, Fatah R, Riches JC, et al. Activated pancreatic stellate cells sequester CD8+ T cells to reduce their infiltration of the juxtatumoral compartment of pancreatic ductal adenocarcinoma. Gastroenterology 2013;145:1121–32. [PubMed: 23891972]
19. Hermann PC, Huber SL, Herrler T, Aicher A, Ellwart JW, Guba M, et al. Distinct populations of cancer stem cells determine tumor growth and metastatic activity in human pancreatic cancer. Cell Stem Cell 2007;1:313–23. [PubMed: 18371365]
20. Shi Y, Gao W, Lytle NK, Huang P, Yuan X, Dann AM, et al. Targeting LIF-mediated paracrine interaction for pancreatic cancer therapy and monitoring. Nature 2019;569:131–5. [PubMed: 30996350]
21. Wang MT, Fer N, Galeas J, Collisson EA, Kim SE, Sharib J, et al. Blockade of leukemia inhibitory factor as a therapeutic approach to KRAS driven pancreatic cancer. Nat Commun 2019;10:3055. [PubMed: 31296870]
22. Lasagni L, Francalanci M, Annunziato F, Lazzeri E, Giannini S, Cosmi L, et al. An alternatively spliced variant of CXCR3 mediates the inhibition of endothelial cell growth induced by IP-10, MIG, and I-TAC, and acts as functional receptor for platelet factor 4. J Exp Med 2003;197:1537–49. [PubMed: 12782716]
23. Loetscher M, Gerber B, Loetscher P, Jones SA, Piali L, Clark-Lewis I, et al. Chemokine receptor specific for IP10 and MIG: structure, function, and expression in activated T-lymphocytes. J Exp Med 1996;184:963–9. [PubMed: 9064356]
24. Cole KE, Strick CA, Paradis TJ, Ogborne KT, Loetscher M, Gladue RP, et al. Interferon-inducible T cell alpha chemoattractant (I-TAC): a novel non-ELR CXC chemokine with potent activity on activated T cells through selective high affinity binding to CXCR3. J Exp Med 1998;187:2009–21. [PubMed: 9625760]
25. Thompson BD, Jin Y, Wu KH, Colvin RA, Luster AD, Birnbaumer L, et al. Inhibition of G alpha i2 activation by G alpha i3 in CXCR3-mediated signaling. J Biol Chem 2007;282:9547–55. [PubMed: 17289675]
26. Lunardi S, Jamieson NB, Lim SY, Griffiths KL, Carvalho-Gaspar M, Al-Assar O, et al. IP-10/CXCL10 induction in human pancreatic cancer stroma influences lymphocytes recruitment and correlates with poor survival. Oncotarget 2014;5: 11064–80. [PubMed: 25415223]
27. Badea L, Herlea V, Dima SO, Dumitrascu T, Popescu I. Combined gene expression analysis of whole-tissue and microdissected pancreatic ductal adenocarcinoma identifies genes specifically overexpressed in tumor epithelia. Hepatogastroenterology 2008;55:2016–27. [PubMed: 19260470]
28. Pei H, Li L, Fridley BL, Jenkins GD, Kalari KR, Lingle W, et al. FKBP51 affects cancer cell response to chemotherapy by negatively regulating Akt. Cancer Cell 2009;16:259–66. [PubMed: 19732725]
29. Sergeant G, van Eijsden R, Roskams T, Van Duppen V, Topal B. Pancreatic cancer circulating tumour cells express a cell motility gene signature that predicts survival after surgery. BMC Cancer 2012;12:527. [PubMed: 23157946]
30. Donahue TR, Tran LM, Hill R, Li Y, Kovochich A, Calvopina JH, et al. Integrative survival-based molecular profiling of human pancreatic cancer. Clin Cancer Res 2012;18:1352–63. [PubMed: 22261810]
31. Zhang G, Schetter A, He P, Funamizu N, Gaedcke J, Ghadimi BM, et al. DPEP1 inhibits tumor cell invasiveness, enhances chemosensitivity and predicts clinical outcome in pancreatic ductal adenocarcinoma. PLoS One 2012;7:e31507.

32. Yang S, He P, Wang J, Schetter A, Tang W, Funamizu N, et al. A novel MIF signaling pathway drives the malignant character of pancreatic cancer by targeting NR3C2. Cancer Res 2016;76:3838–50. [PubMed: 27197190]
33. Cancer Genome Atlas Research Network. Integrated genomic characterization of pancreatic ductal adenocarcinoma. Cancer Cell 2017;32:185–203. [PubMed: 28810144]
34. West S, Kumar S, Batra SK, Ali H, Ghersi D. Uncovering and characterizing splice variants associated with survival in lung cancer patients. PLoS Comput Biol 2019;15:e1007469. [PubMed: 31652257]
35. Patro R, Duggal G, Love MI, Irizarry RA, Kingsford C. Salmon provides fast and bias-aware quantification of transcript expression. Nat Methods 2017;14: 417–9. [PubMed: 28263959]
36. Maurer C, Holmstrom SR, He J, Laise P, Su T, Ahmed A, et al. Experimental microdissection enables functional harmonisation of pancreatic cancer subtypes. Gut 2019;68:1034–43. [PubMed: 30658994]
37. Kramer A, Green J, Pollard J Jr, Tugendreich S. Causal analysis approaches in ingenuity pathway analysis. Bioinformatics 2014;30:523–30. [PubMed: 24336805]
38. Newman AM, Liu CL, Green MR, Gentles AJ, Feng W, Xu Y, et al. Robust enumeration of cell subsets from tissue expression profiles. Nat Methods 2015; 12:453–7. [PubMed: 25822800]
39. Kumar S, Das S, Rachagani S, Kaur S, Joshi S, Johansson SL, et al. NCOA3-mediated upregulation of mucin expression via transcriptional and posttranslational changes during the development of pancreatic cancer. Oncogene 2015;34:4879–89. [PubMed: 25531332]
40. Subramanian A, Tamayo P, Mootha VK, Mukherjee S, Ebert BL, Gillette MA, et al. Gene set enrichment analysis: a knowledge-based approach for interpreting genome-wide expression profiles. Proc Natl Acad Sci U S A 2005;102: 15545–50. [PubMed: 16199517]
41. Deng S, Deng Q, Zhang Y, Ye H, Yu X, Zhang Y, et al. Non-platelet-derived CXCL4 differentially regulates cytotoxic and regulatory T cells through CXCR3 to suppress the immune response to colon cancer. Cancer Lett 2019;443:1–12. [PubMed: 30481563]
42. Dangaj D, Bruand M, Grimm AJ, Ronet C, Barras D, Duttagupta PA, et al. Cooperation between constitutive and inducible chemokines enables T cell engraftment and immune attack in solid tumors. Cancer Cell 2019;35:885–900. [PubMed: 31185212]
43. Wei Y, Lao XM, Xiao X, Wang XY, Wu ZJ, Zeng QH, et al. Plasma cell polarization to the immunoglobulin G phenotype in hepatocellular carcinomas involves epigenetic alterations and promotes hepatoma progression in mice. Gastroenterology 2019;156:1890–904. [PubMed: 30711627]
44. Zhang C, Li Z, Xu L, Che X, Wen T, Fan Y, et al. CXCL9/10/11, a regulator of PD-L1 expression in gastric cancer. BMC Cancer 2018;18:462. [PubMed: 29690901]
45. Kawada K, Hosogi H, Sonoshita M, Sakashita H, Manabe T, Shimahara Y, et al. Chemokine receptor CXCR3 promotes colon cancer metastasis to lymph nodes. Oncogene 2007;26:4679–88. [PubMed: 17297455]
46. Cabrita R, Lauss M, Sanna A, Donia M, Skaarup Larsen M, Mitra S, et al. Tertiary lymphoid structures improve immunotherapy and survival in melanoma. Nature 2020;577:561–5. [PubMed: 31942071]
47. Helmink BA, Reddy SM, Gao J, Zhang S, Basar R, Thakur R, et al. B cells and tertiary lymphoid structures promote immunotherapy response. Nature 2020; 577:549–55. [PubMed: 31942075]
48. Petitprez F, de Reynies A, Keung EZ, Chen TW, Sun CM, Calderaro J, et al. B cells are associated with survival and immunotherapy response in sarcoma. Nature 2020;577:556–60. [PubMed: 31942077]
49. Quemener C, Baud J, Boye K, Dubrac A, Billottet C, Soulet F, et al. Dual roles for CXCL4 chemokines and CXCR3 in angiogenesis and invasion of pancreatic cancer. Cancer Res 2016;76:6507–19. [PubMed: 27634764]
50. Hirth M, Gandla J, Hoper C, Gaida MM, Agarwal N, Simonetti M, et al. CXCL10 and CCL21 promote migration of pancreatic cancer cells toward sensory neurons and neural remodeling in tumors in mice, associated with pain in patients. Gastroenterology 2020;159: 665–81. [PubMed: 32330476]

Translational Relevance

Immunotherapies have failed to produce meaningful improvements in the outcomes of patients with pancreatic ductal adenocarcinoma (PDAC), suggesting a multifaceted nature of immunosuppression in PDAC. Several cytokines and chemokines have a profound influence in both PDAC cell biology and immune response; therefore, we performed a screen to determine differentially expressed cytokine/chemokine genes in 172 PDACs and 126 normal pancreas microarray, The Cancer Genome Atlas dataset, and micro-dissected RNA-sequencing samples. From this screen, CXCR3 ligands, *CXCL9* and *CXCL10*, emerged as highly and consistently overexpressed in PDAC samples. In-depth analyses of this signaling pathway demonstrated that *CXCL9* and *10* are strongly associated with poor overall survival in patients with PDAC, and associate with altered immune cell infiltrates, specifically, T-cell exhaustion gene signatures. Cumulatively, our findings suggest that activation of CXCR3 signaling is a novel immunosuppressive pathway in PDAC that is distinct from established checkpoint mechanisms.

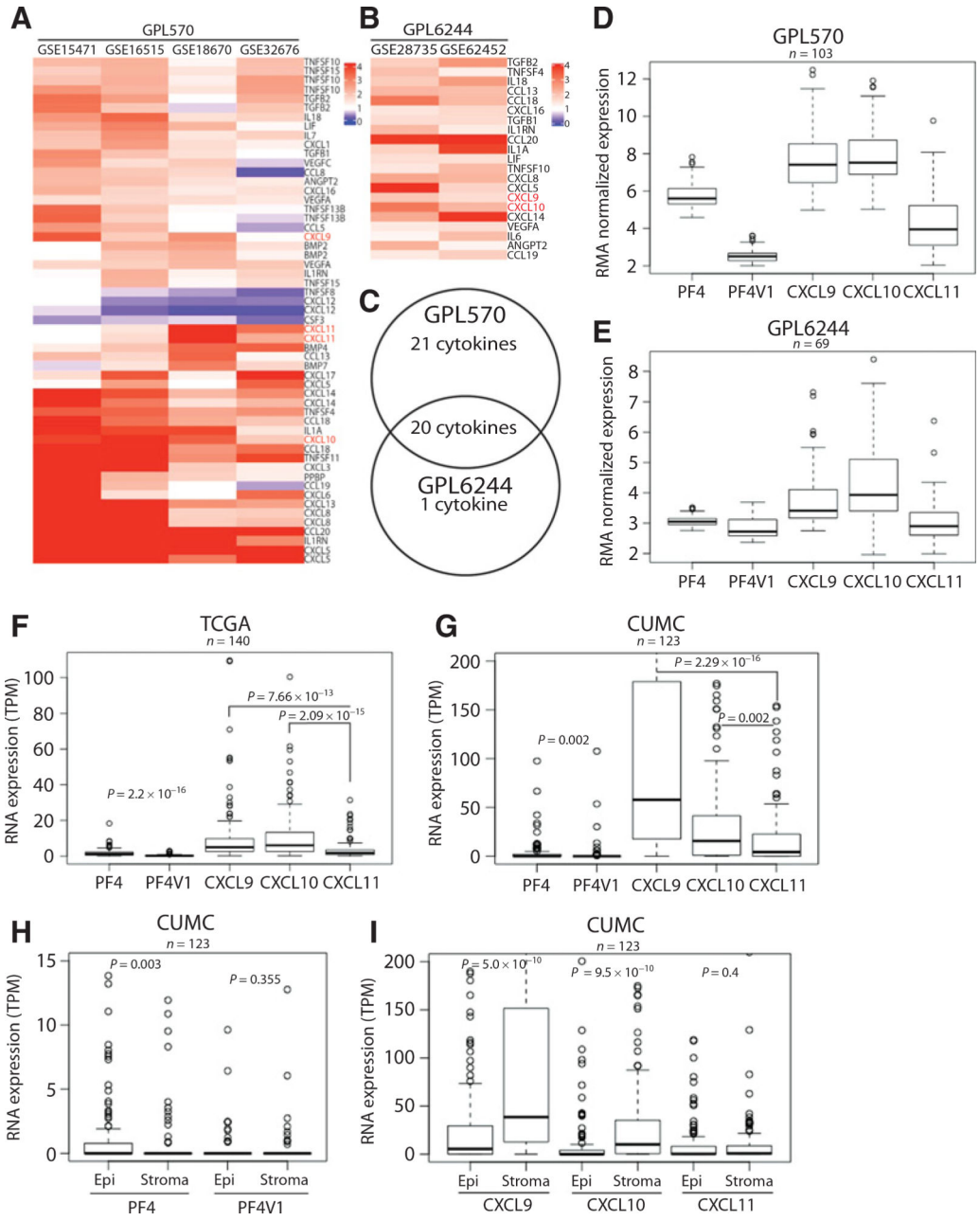

Figure 1.

Expression profile of cytokines in PDAC. **A** and **B,** Heatmap of mean cytokine expression in PDAC relative to normal in GPL570 and GPL6244 arrays, respectively; cytokines with mean expression higher than 1.5-fold or less than 0.75-fold are depicted. **C,** Venn diagram depicting overlap in identified cytokines between GPL570 and GPL6244 arrays. **D**–**G,** Expression profiles of all CXCR3 ligands in GPL570 and GPL6244 microarray datasets, PDAC samples in the PAAD TCGA dataset, and total cytokine expression from CUMC RNA-seq dataset, respectively. **H** and **I,** Distributions of CXCR3 ligand expression in epithelial and stromal compartments from CUMC-paired micro-dissected samples. The *P* values were generated by the Mann–Whitney U test.

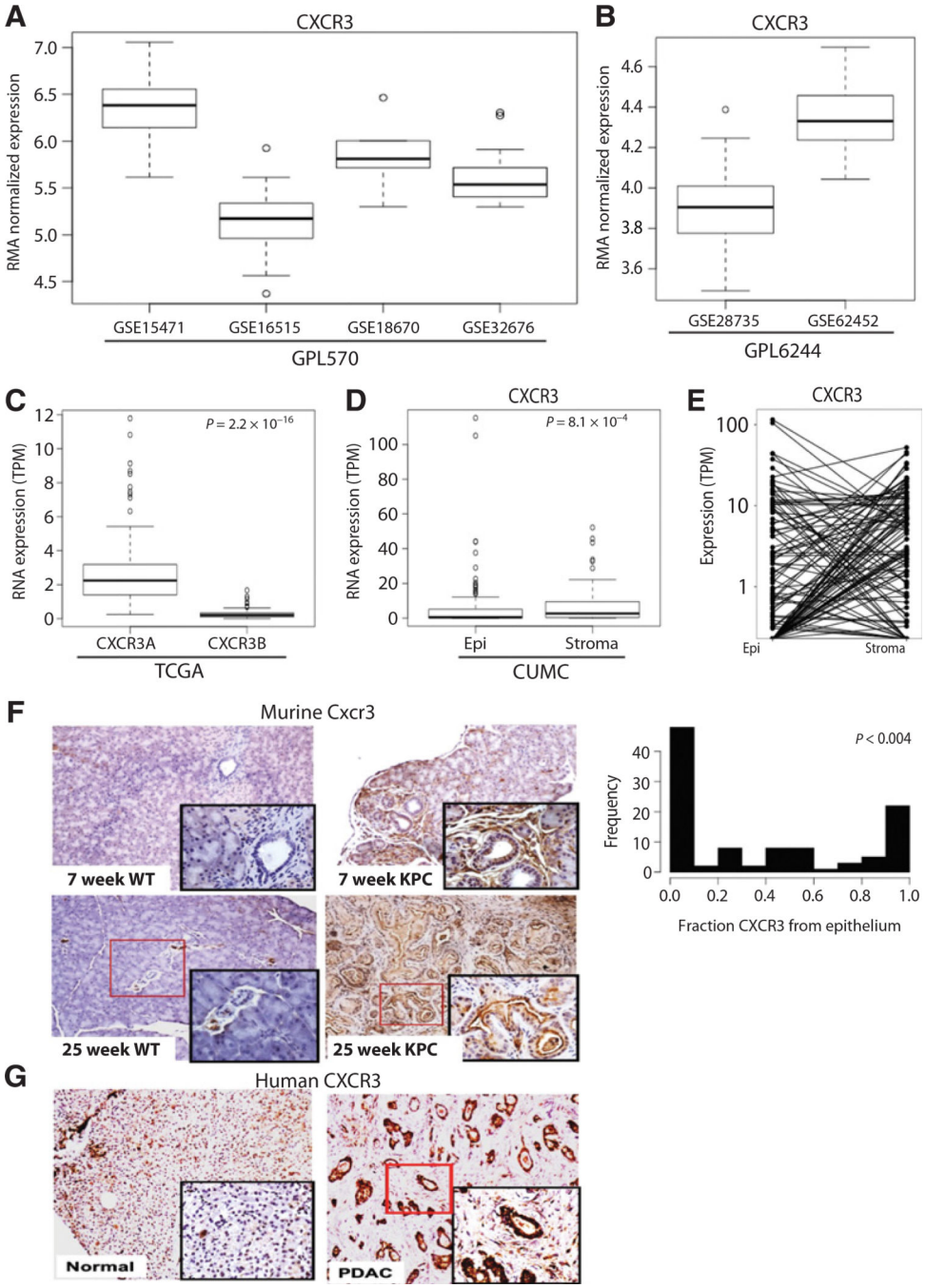

Figure 2.

CXCR3 is expressed in PDAC tissue. **A** and **B,** Expression of *CXCR3* in GPL570 and GPL6244 arrays normalized with robust multi-array average. **C,** Expression of *CXCR3* splice variants, *CXCR3A* and *B*, based on transcript reconstruction from PDAC samples in TCGA data. **D,** Distribution of *CXCR3* expression in epithelial and stromal compartments and total expression in CUMC data. The *P* values for **A–C** were generated by Mann–Whitney U test. **E,** Jaccard plot of expression of *CXCR3* expression in paired epithelial and stromal samples, and histogram of fractional expression of *CXCR3* (*P* value generated by

10,000 iterations of data randomization and comparison of a number of randomized samples with a single-source expression of *CXCR3* to that of the actual expression set). **F,** IHC of CXCR3 expression in the KPC progression model of PDAC at 7 and 25 weeks, with pancreas from WT littermates for controls. **G,** IHC of CXCR3 expression in human normal and PDAC samples.

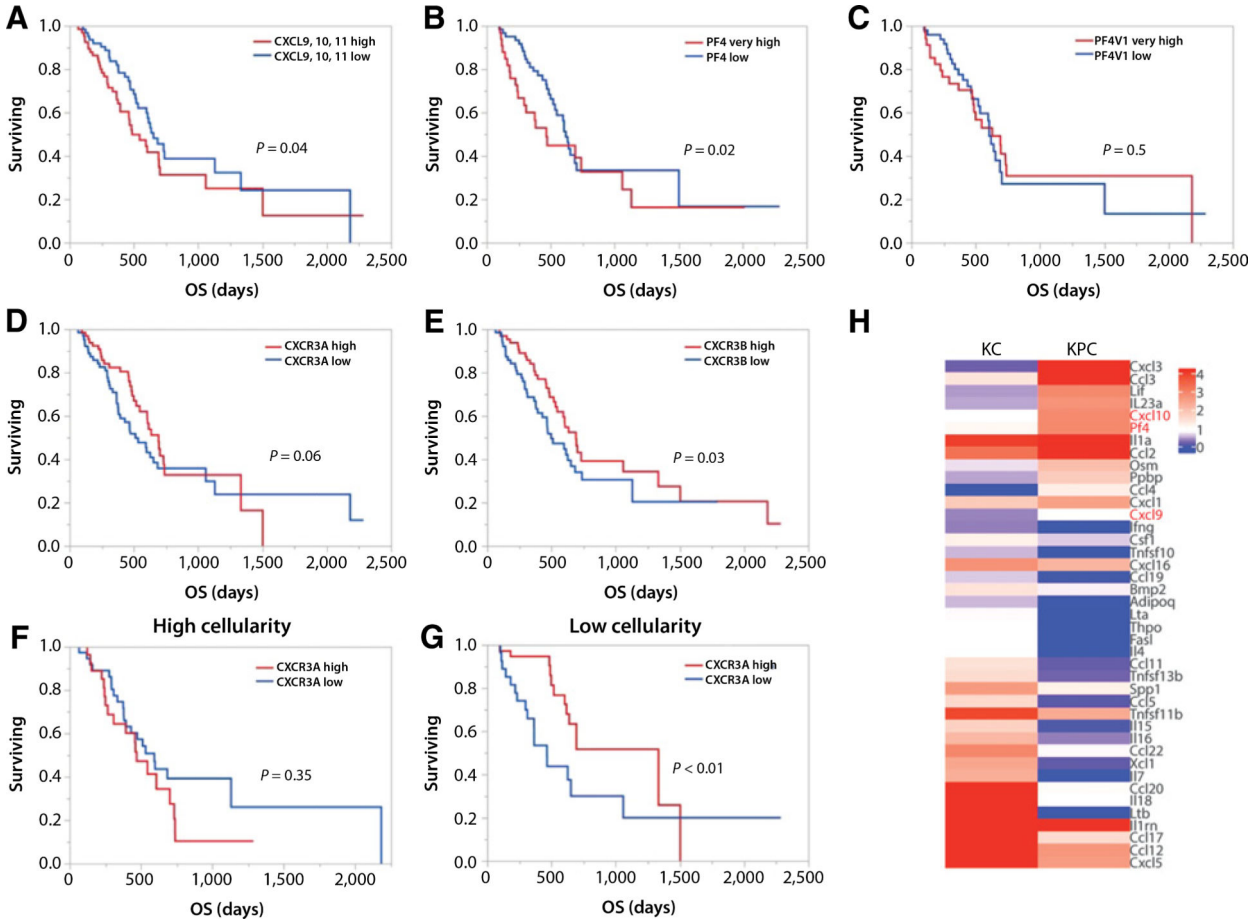

Figure 3.

Expression levels of CXCR3 and its ligands are associated with OS in human and murine PDAC. **A** and **B**, Kaplan–Meier plots of OS of patients with PDAC in PAAD TCGA datasets stratified by median expression of combined *CXCL9, CXCL10*, and *CXCL11* expression (**A**) and 75th percentile of *PF4* expression compared with the bottom 50% of *PF4* expressers (**B**). **C**, Kaplan–Meier plot of OS in patients stratified by 75th percentile of *PF4V1* expression compared with bottom 50% of expressers. **D** and **E,** Kaplan–Meier plots of OS in patients stratified by median *CXCR3A* and *B* expression, respectively. **F** and **G,** Kaplan–Meier plots of OS in patients stratified by median *CXCR3A* expression in high- and low-cellularity patient subgroups (defined by median cellularity). **H,** Heatmap depicting results of qRT-PCR array of cytokine expression in KC and KPC pancreas relative to expression in WT littermates; entries are ranked in descending order by the difference in FC between KC and KPC. The *P* values were generated by the Wilcoxon test.

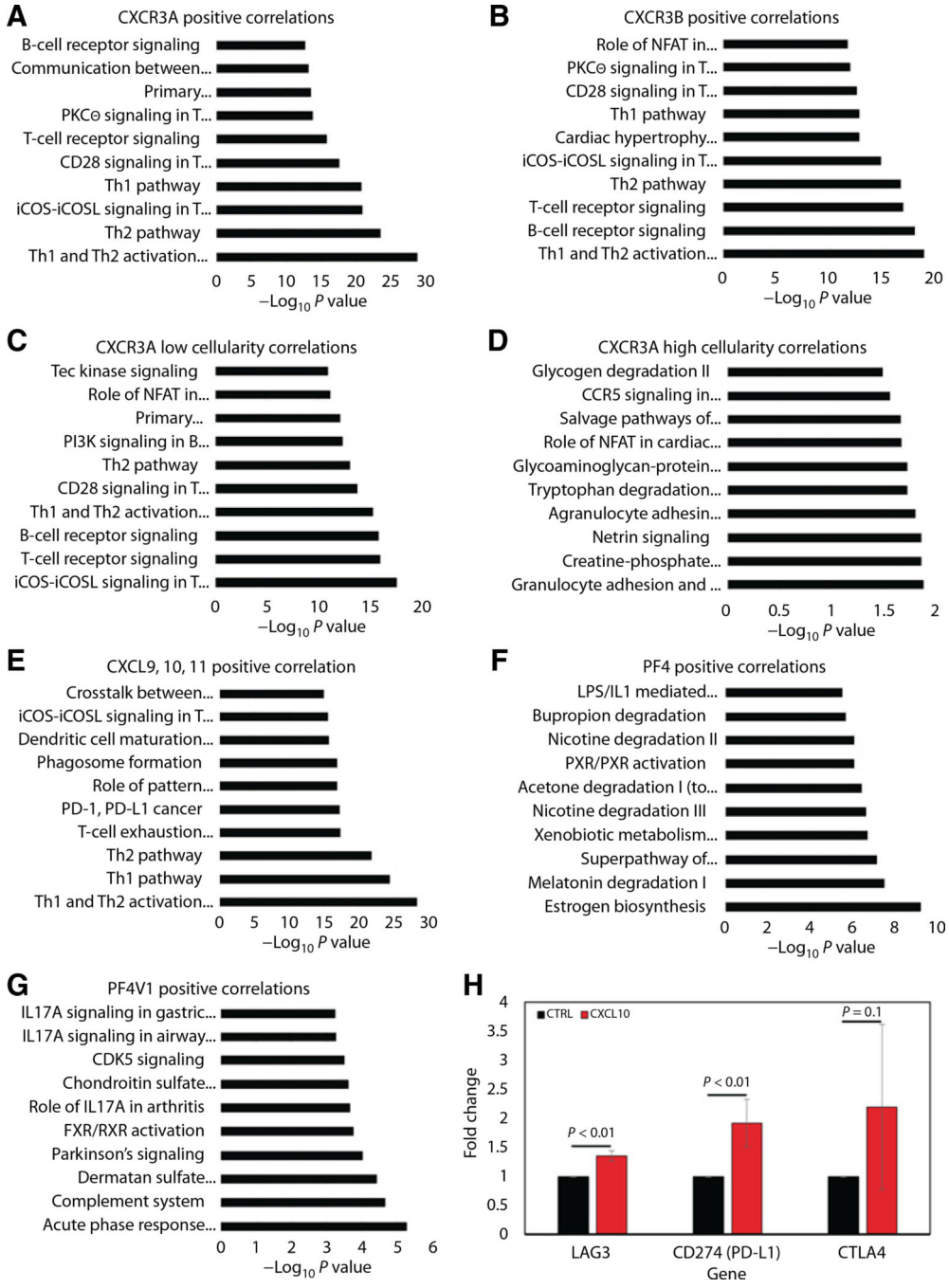

Figure 4.

CXCR3 expression is correlated with a T-cell–related gene signature, while *CXCL9, 10*, and *11* are correlated with T-cell– and T-cell exhaustion–related signatures. **A** and **B,** IPA results for genes highly correlated (rho > 0 and $P < 0.001$) with *CXCR3A* and *B* expression in TCGA data. **C** and **D,** IPA results for genes correlated with *CXCR3A* in low- and high-cellularity samples, respectively. **E–G**, IPA results for genes highly correlated with *CXCL9, 10*, and *11*; *PF4*; and *PF4V1* expression, respectively, in TCGA data. Gene sets selected on the basis of Spearman rho correlations; *P* values for IPA analysis were generated by IPA. **H,**

The qRT-PCR analysis of *ex vivo* murine splenocytes treated with vehicle control or *Cxcl10* for markers of immunosuppression.

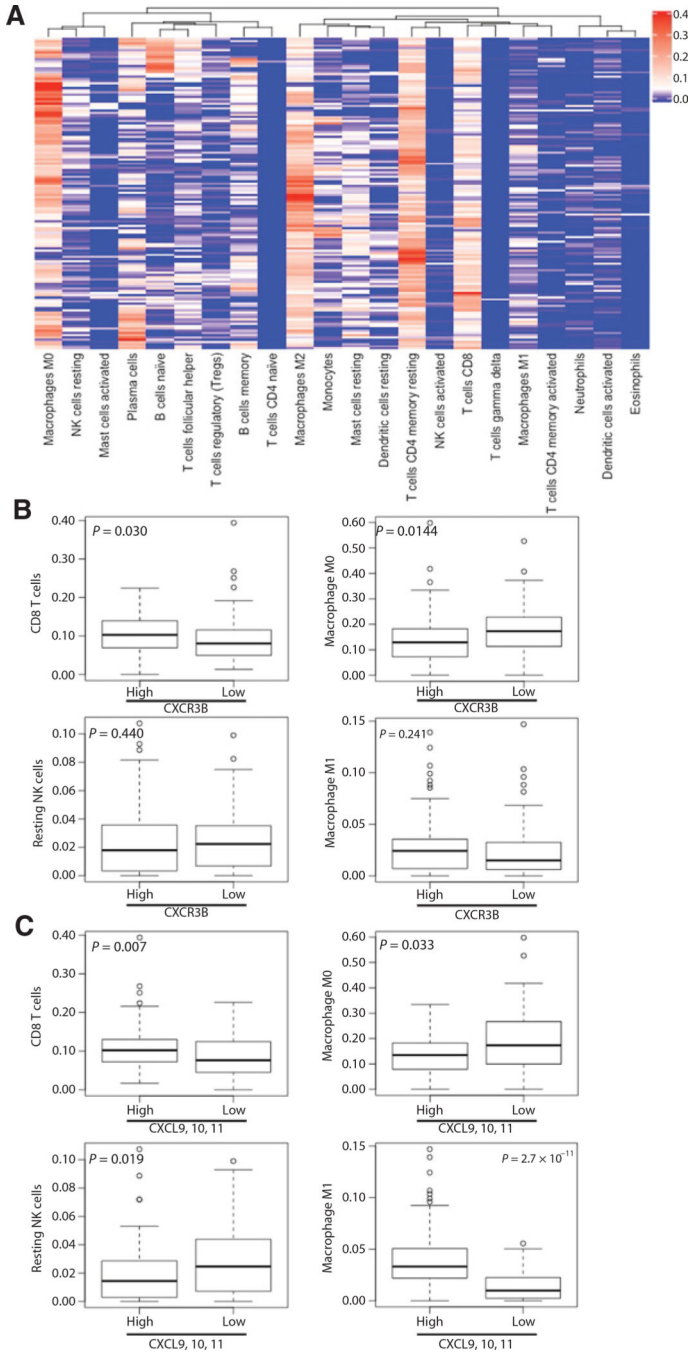

Figure 5.

Expression of *CXCR3* and CXCR3A ligands is associated with changes in CIBERSORT immune cell signatures. **A,** Heatmap depicting the distributions of immune cell expression signatures derived from the LM22 gene expression signature matrix in TCGA PDAC patient expression data. **B,** Box plots depicting the distribution of CD8 T cell, macrophage Mθ, resting NK cell, and macrophage M1 signatures in *CXCR3B*-high and -low groups (defined by median) in TCGA data. **C,** Box plots depicting the distribution of CD8 T cell, macrophage Mθ, resting NK cell, and macrophage M1 signatures in *CXCL9, 10*, and *11*–

high and –low groups (defined by median) in TCGA data. The *P* values were calculated by the Mann–Whitney U test.

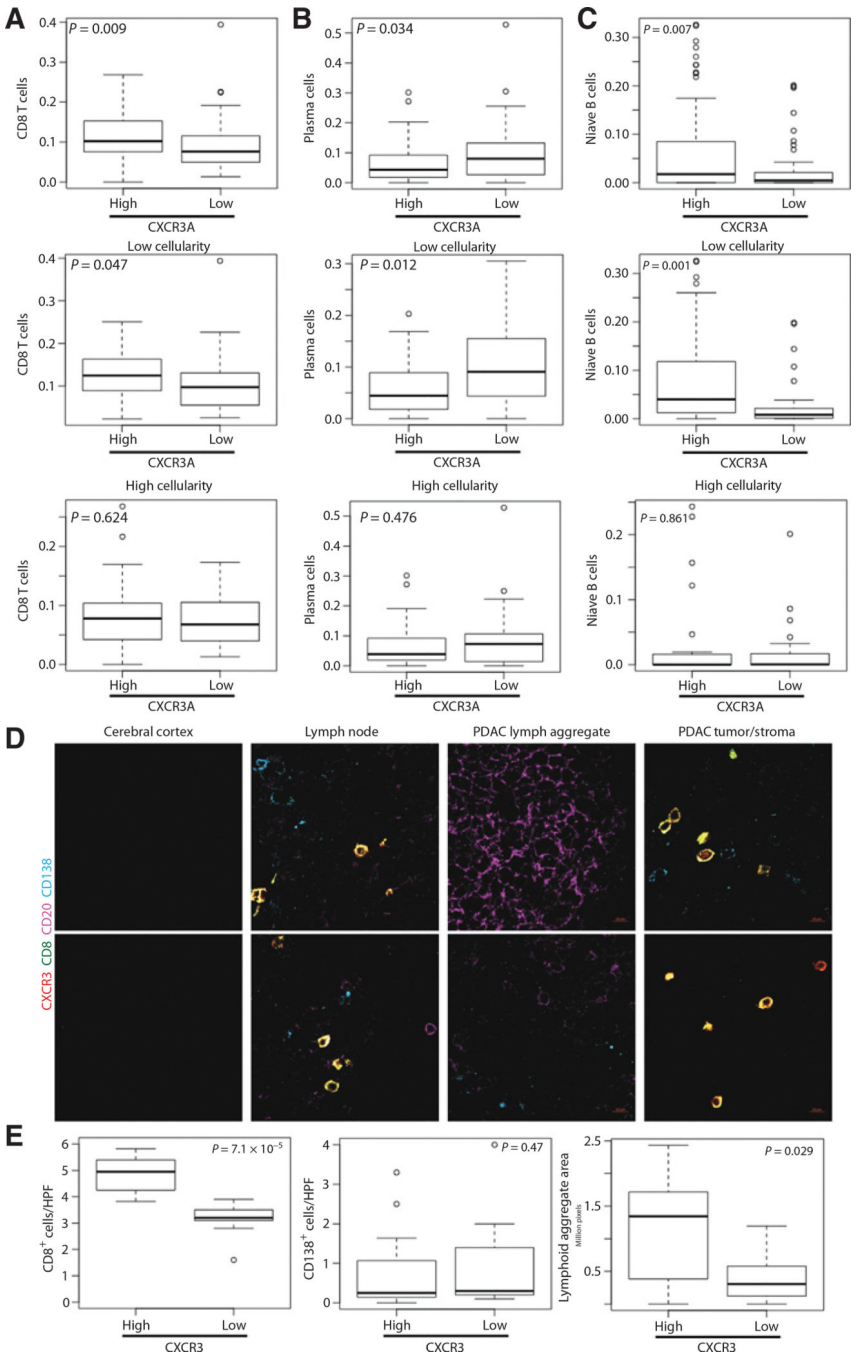

Figure 6.

CIBERSORT changes were associated with *CXCR3A* expression only in the low-cellularity patient subset. **A,** Box plots depicting the distribution of CIBERSORT CD8 T-cell signature from TCGA data in *CXCR3A*-high and -low groups as defined by the median in the total population (top), the low-cellularity subgroup of samples (middle), and high-cellularity subgroup (bottom). **B,** Box plots depicting the distribution of CIBERSORT plasma cell signature from TCGA data in *CXCR3A*-high and -low groups as defined by the median in the total population (top), the low-cellularity subgroup of samples (middle), and the high-

cellularity subgroup (bottom). **C,** Box plots depicting the distribution of CIBERSORT naïve B-cell signature from TCGA data in *CXCR3A*-high and -low groups as defined by the median in the total population (top), low-cellularity subgroup (middle), and high-cellularity subgroup (bottom). **D,** Representative images of IF staining for CXCR3 (red), CD8 (green), CD20 (magenta), and CD138 (cyan) of human controls and PDAC tissue samples. **E,** Box plots depicting the distribution of mean number of $CD8^+$ and $CD138^+$ cells per high power field and total lymphoid aggregate area in PDAC samples with high and low CXCR3 expression. The *P* values were calculated by the Mann–Whitney U test.